Supplement of Atmos. Meas. Tech., 16, 529–546, 2023
https://doi.org/10.5194/amt-16-529-2023-supplement
© Author(s) 2023. CC BY 4.0 License.

Atmospheric Measurement Techniques
Open Access
EGU

Supplement of

Field comparison of two novel open-path instruments that measure dry deposition and emission of ammonia using flux-gradient and eddy covariance methods

Daan Swart et al.

Correspondence to: Susanna Rutledge-Jonker (susanna.jonker@rivm.nl)

The copyright of individual parts of the supplement might differ from the article licence.

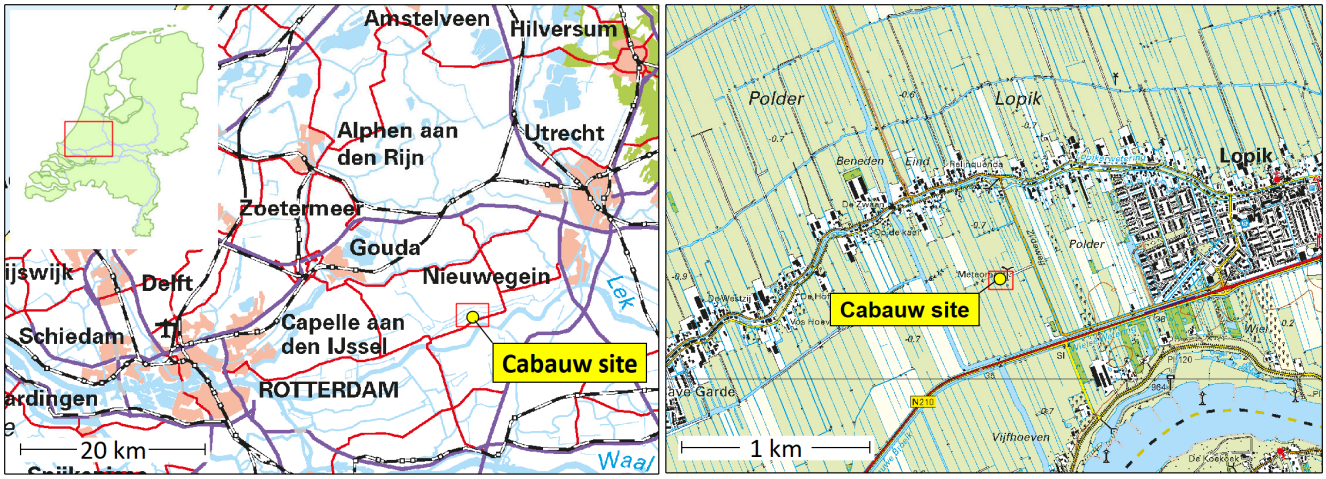

Figure S1. The location of Cabauw in the Netherlands. Maps from www.pdok.nl/ (downloaded 07-02-2021).

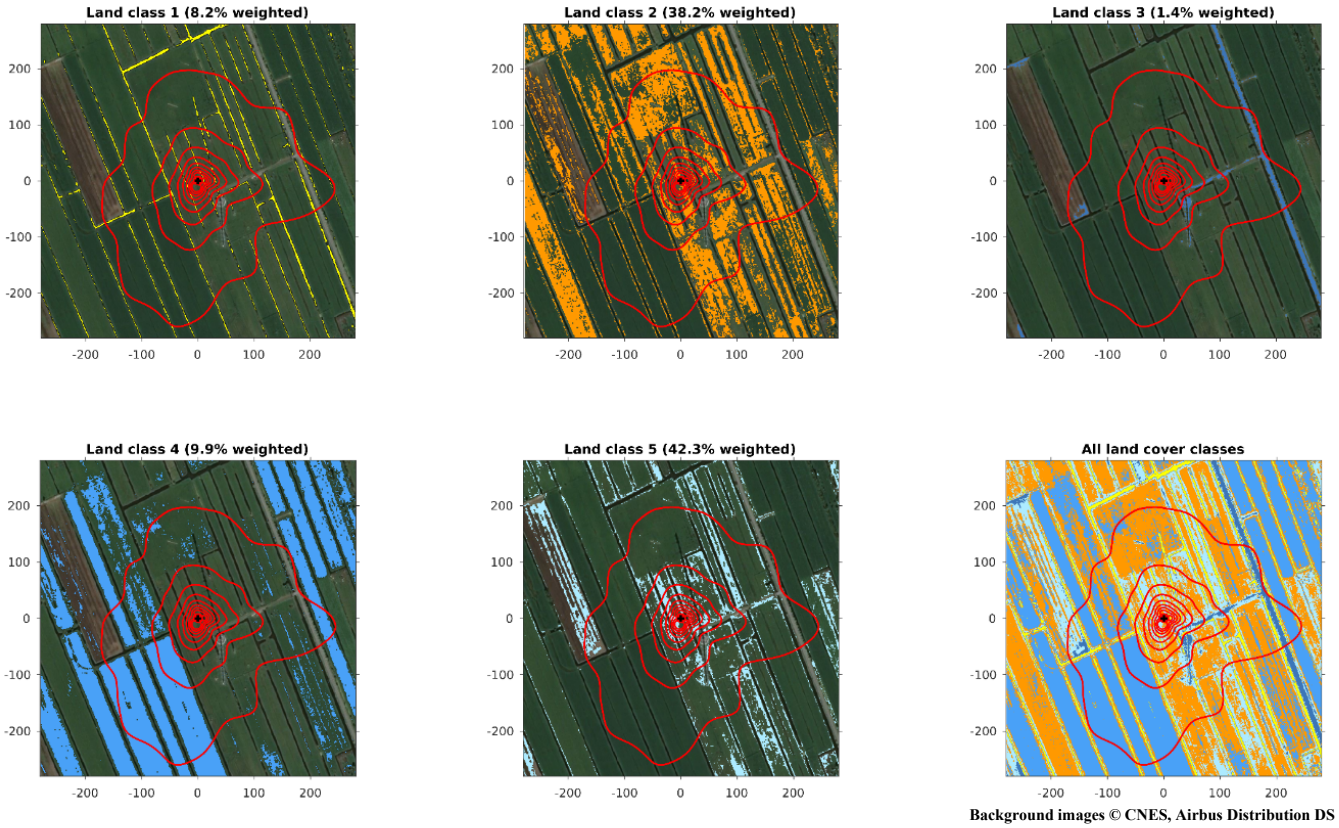

Figure S2. Unsupervised land cover classification based on Google Map (RGB) images, derived using Flux Footprint Predictions (https://geography.swansea.ac.uk/nkljun/ffp/www/). Five land cover classes and their individual distribution ratios under the EC footprint area are shown. The following land covers were defined (in order of increasing percentage of the footprint area):
Land class 5: wet grassland, in light blue (count 42.3%);
Land class 2: less wet grassland, in orange (count 38.2%);
Land class 4: hay land (harvested grassland), in bright blue (count 9.9%);
Land class 1: ditches and drainage lines, in light yellow (count 8.2%);
Land class 3: concrete road surface, in dark blue (count 1.4%).
Land classes 5 and 2 have a similar roughness height, while land class 4 has lower roughness. Background map data: Microsoft, CNES Distribution Airbus DS.

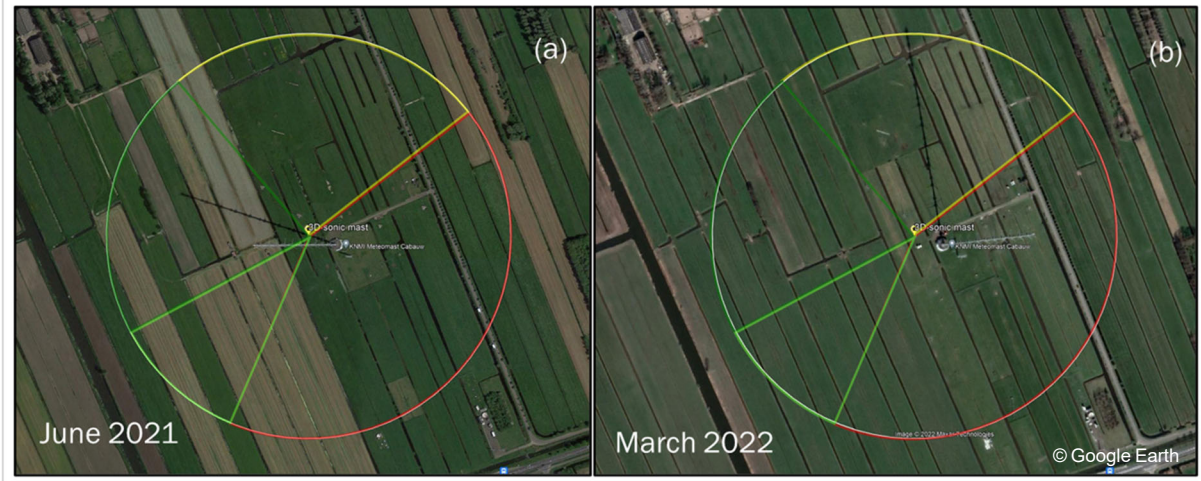

Figure S3. ©Google Earth image of the land cover within a 300-meter radius in June 2021 (a); idem in March 2022 (b).

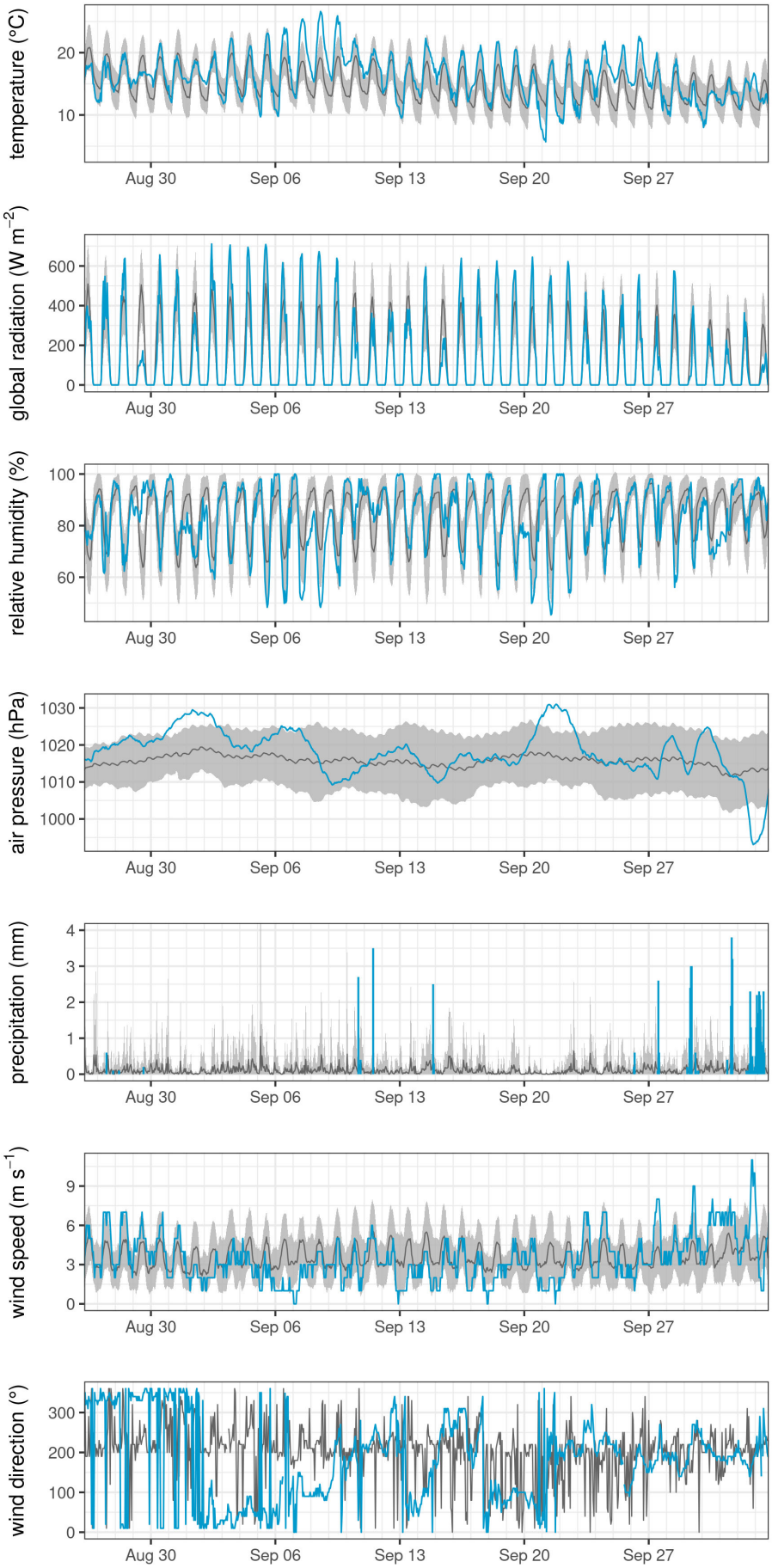

Figure S4. The weather conditions during the measurement campaign (blue lines) as observed by the KNMI automated weather station (hourly averages). The grey lines represent the average weather conditions of the past 30 years (1991-2020), and the grey area the corresponding standard deviation. For the wind direction, the mode (most frequently occurring wind direction) of the past 30 years is plotted.

1.1 ICO method quality control

To ensure the quality of the half-hourly damping correction factors of the ICO method, values were filtered according to the following criteria: QC flag 0 in Eddy Pro (Mauder and Foken, 2006); $u_* > 0.1$ m s^{-1}; the variances in the NH_3 concentration are below 2 times the standard deviation plus the mean of the overall campaign period; EddyPro found a maximum in the covariance within the prescribed time lag window. In total, 661 half-hour NH_3 correction factors were left for correcting their respective fluxes. If half-hourly corrections factors were not available due to quality criteria, we used daily medians to correct corresponding fluxes.

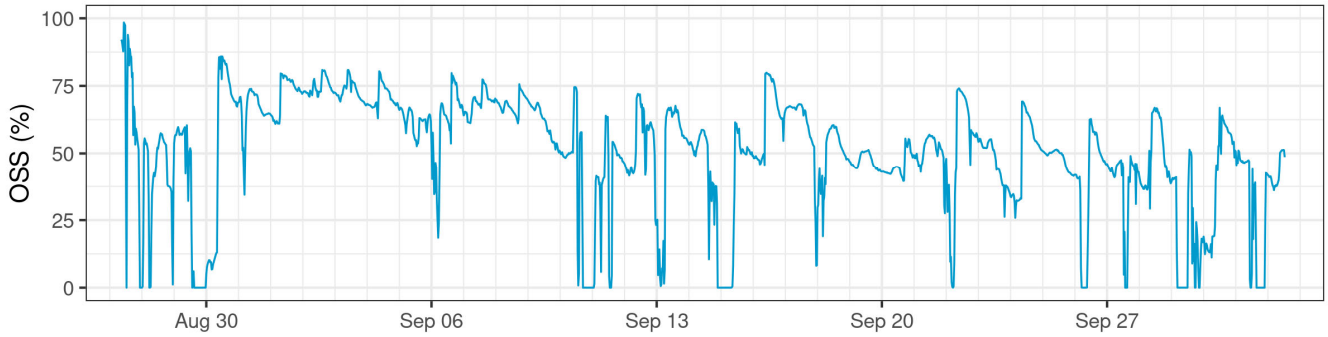

Figure S5. Optical signal strength (OSS) of the HT instrument during the measurement campaign.

1.2 Uncertainty analysis

The random error of the half-hourly AGM NH_3 fluxes ($\sigma_{F_{AGM,}}$) has three error components and was estimated as follows:

$$\sigma_{F_{AGM}} = |F_{NH_3}| \sqrt{\left(\frac{\sigma_{u_*}}{u_*}\right)^2 + \left(\frac{\sigma_{c_{NH_3}(z_2) - c_{NH_3}(z_1)}}{c_{NH_3}(z_2) - c_{NH_3}(z_1)}\right)^2 + \left(\frac{\sigma_{f(z,\Psi)}}{f(z,\Psi)}\right)^2} \quad \text{Eq. S1}$$

Here, the three error components are:

1. the relative error of the u_* values, $\frac{\sigma_{u_*}}{u_*}$,
2. the relative error of the difference in the miniDOAS NH_3 concentration at height z_1 and z_2, $\frac{\sigma_{c_{NH_3}(z_2) - c_{NH_3}(z_1)}}{c_{NH_3}(z_2) - c_{NH_3}(z_1)}$,
3. and an error term related to the stability correction at each measurement height, $\frac{\sigma_{f(z,\Psi)}}{f(z,\Psi)}$, with $f(z,\Psi) = \ln\left(\frac{z_2}{z_1}\right) - \Psi_H\left(\frac{z_2}{L}\right) + \Psi_H\left(\frac{z_1}{L}\right)$.

The relative errors of the u_* are estimated in EddyPro following Finkelstein and Sims (2001). The relative error of the miniDOAS NH_3 concentration differences is determined to be 0.088 µg m^{-3} during the cross periods (see Sect. 4.1.1). Finally, we assumed that the errors in the height of the measurements (z_1 and z_2) were negligible and that the error in $f(z,\Psi)$ solely depends on the errors in the stability corrections. Following Wolff et al. (2010), we assumed that the stability corrections have a relative error of 10%.

The random error of the half-hourly uncorrected EC NH_3 fluxes is estimated in EddyPro following Finkelstein and Sims (2001). The random error of the WPL corrected NH_3 fluxes, is computed as follows whereby Eq. 2 is rewritten as a sum of four terms F_1, F_2, F_3 and F_4:

$$F_{EC} = A\overline{w'\rho_A'} + AB\mu\frac{\overline{\rho_A}}{\overline{\rho_d}}\overline{w'\rho_v'} + AC\frac{\overline{\rho_A}}{\overline{T_a}}\overline{w'T_a'} + AC\mu\frac{\overline{\rho_v}}{\overline{\rho_d}}\frac{\overline{\rho_A}}{\overline{T_a}}\overline{w'T_a'} = F_1 + F_2 + F_3 + F_4 \quad \text{Eq. S2}$$

The random error of the WPL method corrected NH_3 fluxes ($\sigma_{F_{NH_3,HT}}$) is computed as follows:

$$\sigma_{F_{EC}} = \sqrt{{\sigma_{F_1}}^2 + {\sigma_{F_2}}^2 + {\sigma_{F_3}}^2 + {\sigma_{F_4}}^2} \quad \text{Eq. S3}$$

Here, the term F_1 represents the NH_3 flux term in the WPL correction, whose random error (σ_{F_1}) largely follows the random error of the HT NH_3 fluxes ($\overline{w'\rho_A'}$) from EddyPro. The term F_2 represents the water vapour term, and F_3 and F_4 together are the heat terms in the WPL correction. To determine the random error of each term, the relative errors of the included variables are propagated. The relative error of the NH_3 density (ρ_A) from the HT reported by the manufacturer is 15% (Wang et al., 2021). The relative errors of the dry air density $\overline{\rho_d}$, water vapor density $\overline{\rho_v}$ and air temperature $\overline{T_a}$ from sonic #1 are estimated to be 5%, 5%, and 1%, respectively (Li-Cor Inc, 2022). Finally, the relative random errors of the water vapour flux ($\overline{w'\rho_v'}$) and the sensible heat flux ($\overline{w'T_a'}$) were taken from EddyPro.

1.3 MiniDOAS intercalibration

The concentration differences between the miniDOAS paths during the three cross periods are shown in Figure S6**.** The blue elements of the time series meet the selection criteria mentioned above. For these blue data points, statistics are given separately for the three periods.

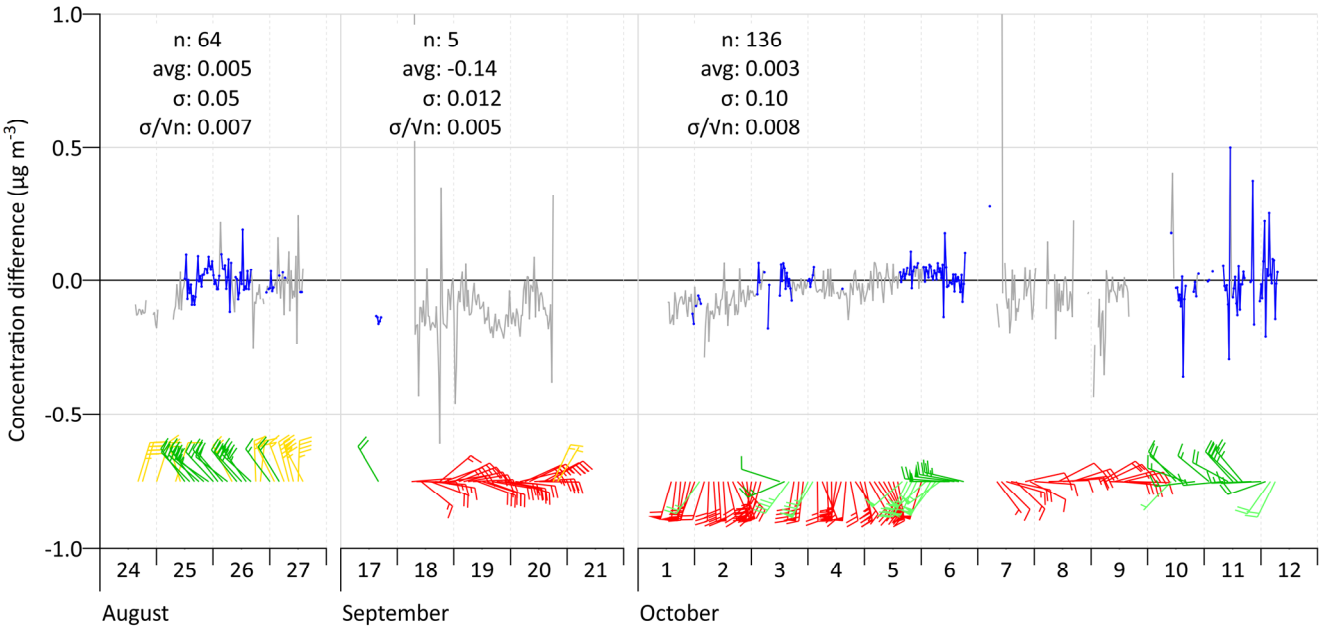

Figure S6. Top trace: Time series of de observed NH_3 concentration difference between the two miniDOAS instruments during the three cross periods, after correction of the top miniDOAS values based on the intercalibration as described in the text. Only data during well-mixed conditions ($u_* > 0.1$ m s^{-1}) are shown. Measurements from obstacle-free wind directions are blue, other directions are grey. The sets of statistics given in the plots apply to the blue measurements only. Bottom trace: 30-minute wind vectors colour-coded with the wind sectors described earlier. Wind speed is indicated as barbs, as used on meteorological maps. To reduce clutter, only 1 in 4 wind vectors are shown.

In the first cross-period, the average half-hourly difference was 0.005 ± 0.007 µg m^{-3} and the standard deviation was 0.05 µg m^{-3} ($n = 64$). For the last cross-period, these values were 0.003 ± 0.008 µg m^{-3} and 0.10 µg m^{-3} ($n = 136$), respectively. The average only shifted by 0.002 µg m^{-3} between cross-periods 1 and 3. This is well within the combined uncertainty range. The spread of the half-hourly values has increased from 0.05 in cross-period 1 to 0.10 µg m^{-3} in cross-period 3. This increase was likely at least partially caused by the gradual decay of the lamp intensity, causing a larger measurement error. The 'ageing' of the field reference spectrum may also have played a role here, but this was not studied further. The conclusion is that, over the full campaign period, the zero-level of the difference measurement has been stable, and the individual difference measurements showed a typical spread of 0.1 µg m^{-3} or less.

The second cross-period contained almost no valid data points, as the wind during this cross-period was coming from the direction of the largest obstacle of all: the 213-meter mast. Its impact on the analysis above was therefore almost zero. The data during this cross-period show how large the magnitude of the effect of upwind obstacles can be. The grey points taken during this cross-period differed systematically from zero by about 0.2 µg m^{-3}, reflecting that the gradients were different at different locations along the paths.

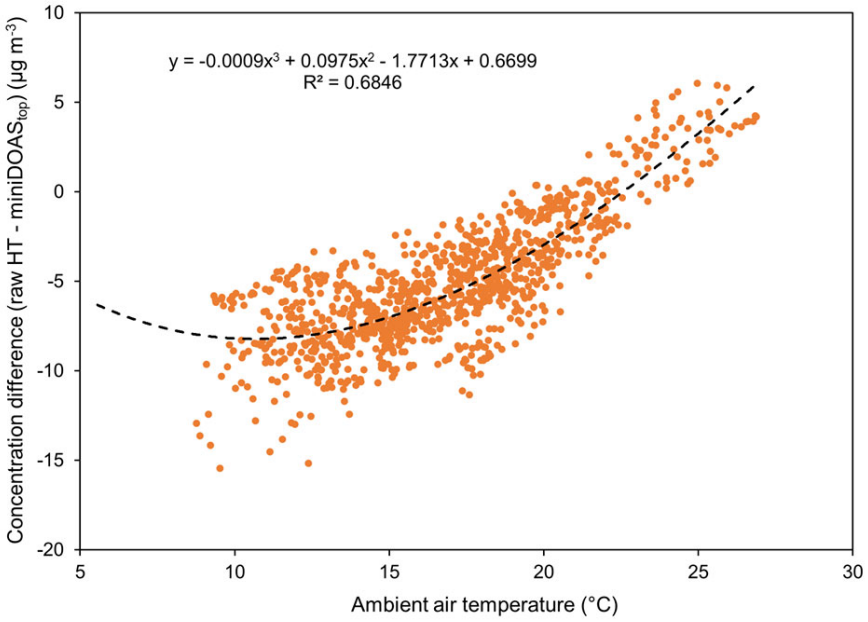

Figure S7. HT concentrations offset (after comparing with miniDOAS$_{top}$) correlation with ambient air temperature.

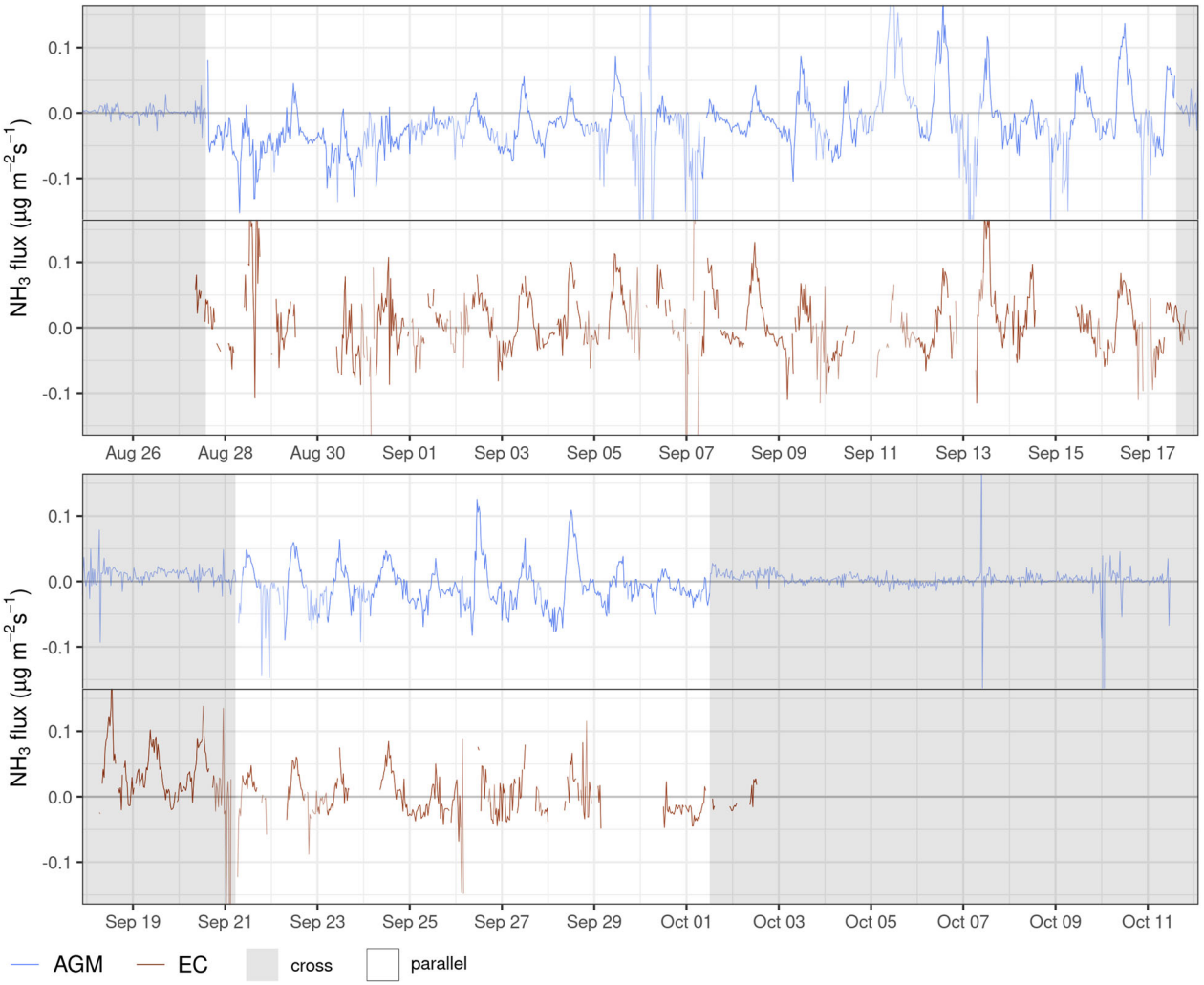

Figure S8. Full time series of the AGM (a) and EC (b) NH_3 fluxes. The grey areas depict measurement periods used for inter-instrumental calibration of the miniDOAS$_{bottom}$ and miniDOAS$_{top}$ (i.e. cross-periods). The transparent lines either indicate measurement during low-mixing conditions ($u_* < 0.1$ m s^{-1}) or outliers.

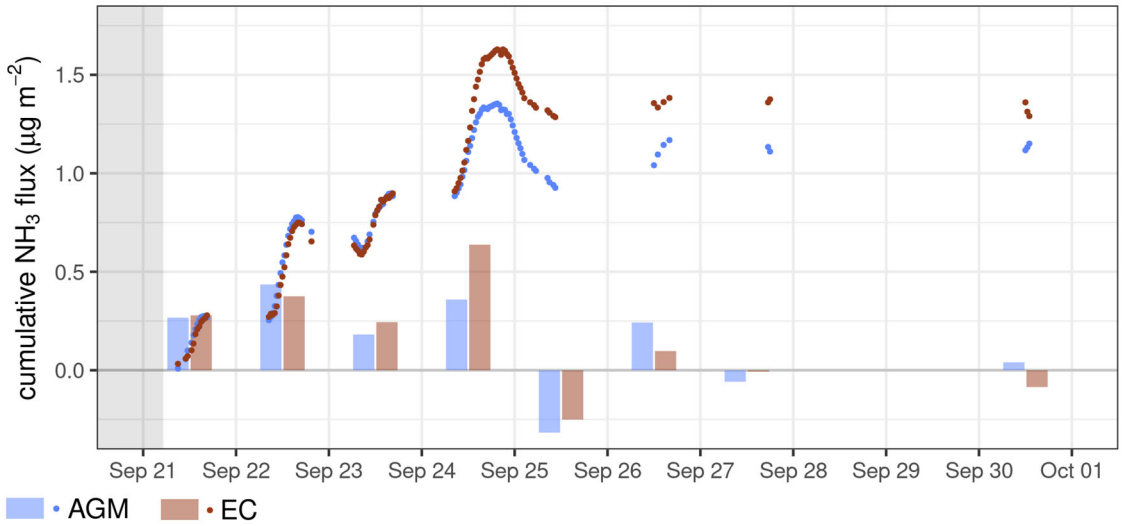

Figure S9. Cumulative EC and AGM NH_3 flux for the period after cross-period 2. Here, filtered NH_3 fluxes from only the green and light green wind directions where both systems have a valid flux observations were used. The bars represent the daily totals per system.

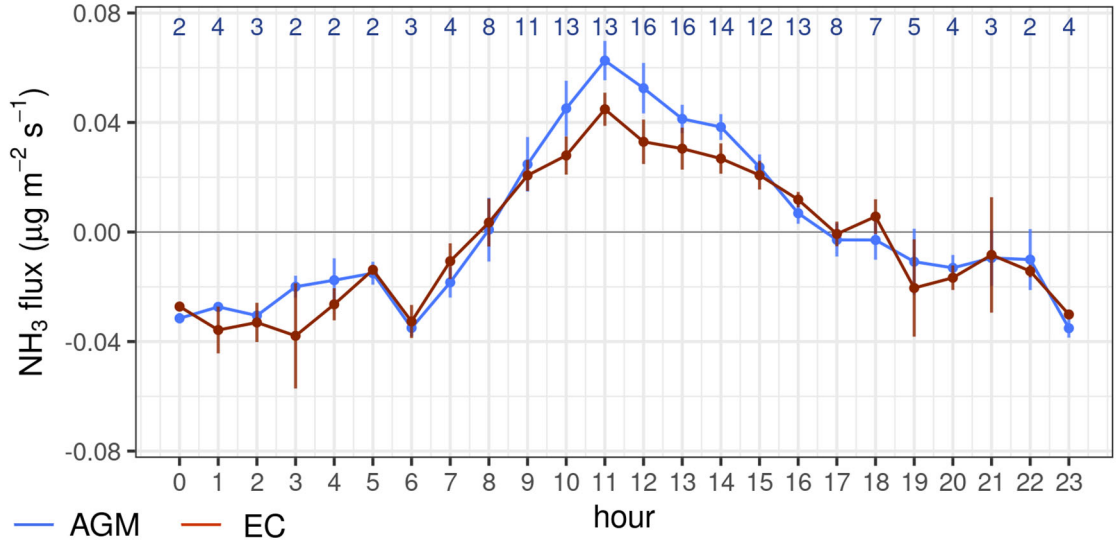

Figure S10. Mean diurnal cycle of the AGM and EC NH_3 flux. Only measurements after September 15 are included, when manure application was not allowed anymore. The error bars indicate the standard error of the hourly mean $(\sigma/\sqrt{n})$. The number of hours averaged (n) are listed in blue text at the top. Here, filtered NH_3 fluxes from only the green and light green wind directions where both systems have a valid flux observation were used.

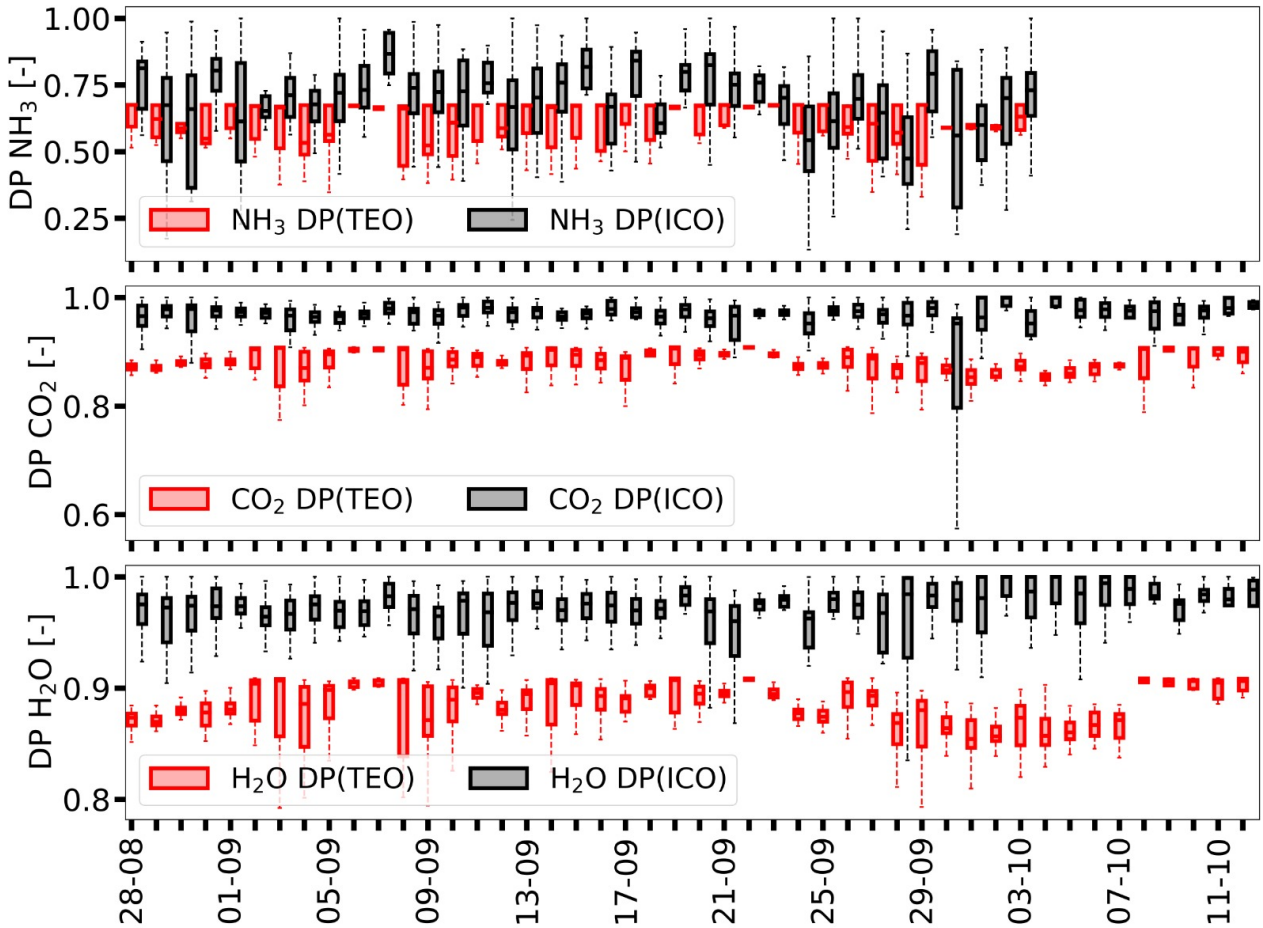

Figure S11. Box-and-whisker plots (box frame = 25 % to 75 % interquartile range (IQR), bold line = median, whisker = 1.5*IQR) of EddyPro theoretical method (TEO) and ICO experimental method calculated damping factors (DP) for NH_3, CO_2 and H_2O flux, respectively.

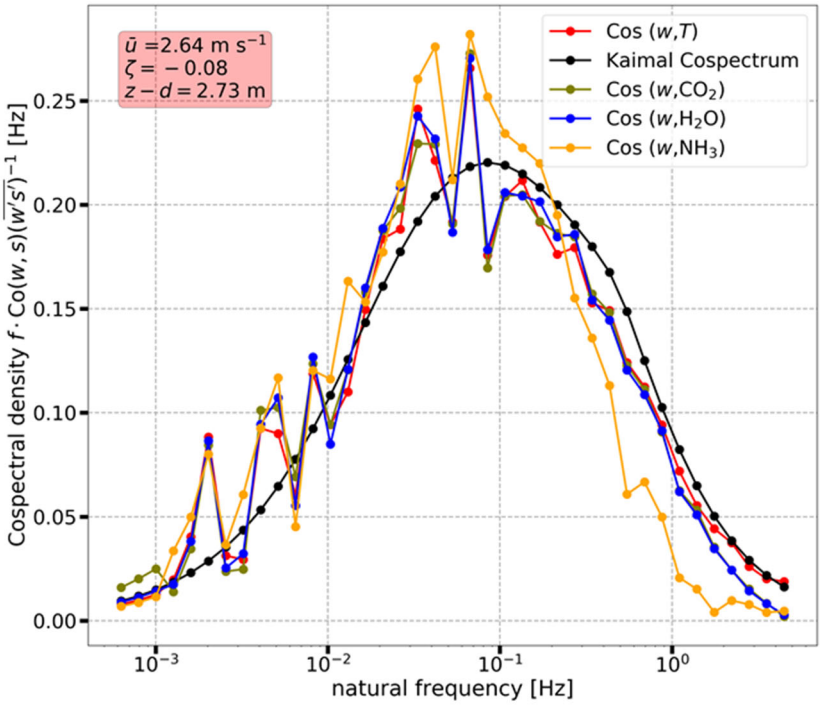

Figure S12. Normalized cospectra of temperature (red), NH_3 (orange), CO_2 (olive), and H_2O (blue) differentiated by their respective colours. Shown cospectra were averaged from 19 September 08:00 to 19 September 12:30. In the red box, average wind speed ($\overline{u}$) and stability (ζ) are shown. Values were used to derive the Kaimal Cospectrum (black).

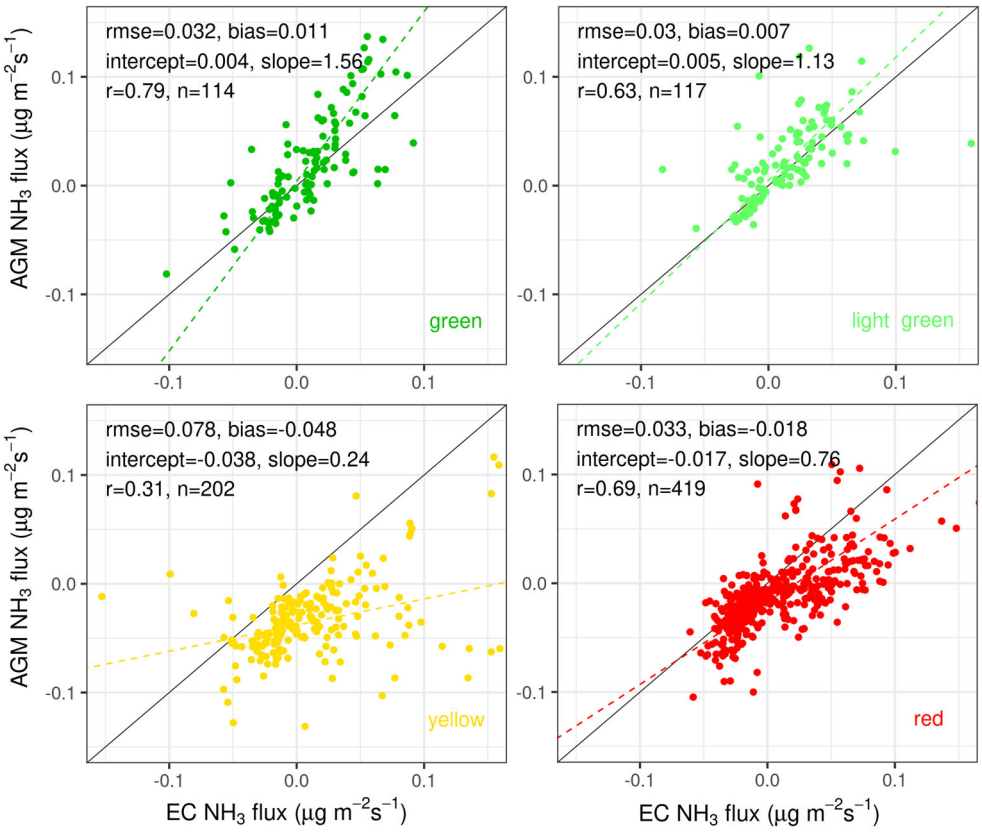

Figure S13. Comparison of the AGM NH_3 fluxes from the miniDOAS instruments and the EC NH_3 fluxes from the HT per categorised wind direction with ICO spectral correction method.

120

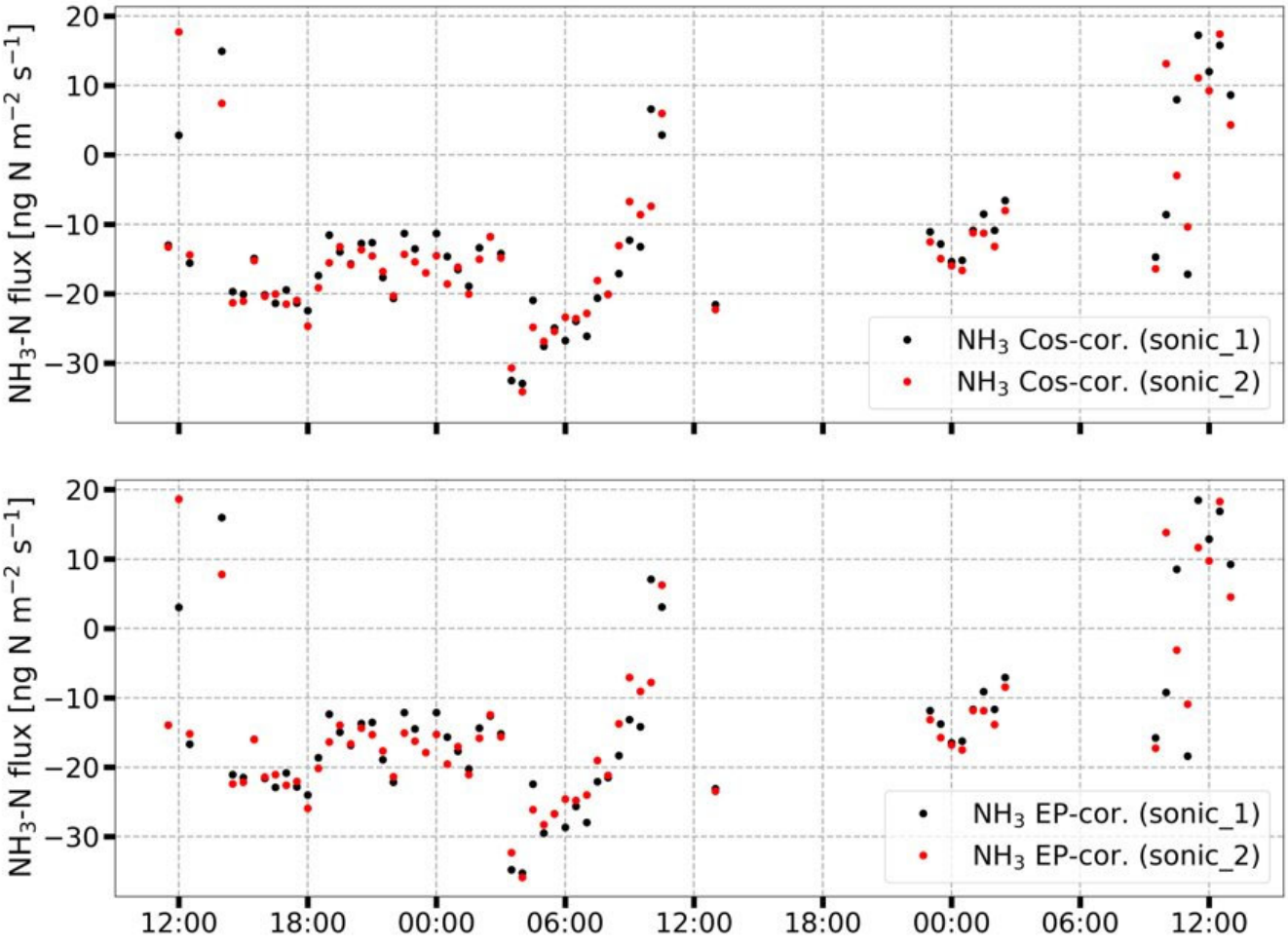

Figure S14. The NH_3 flux computed with the EC method using vertical wind component measurements from either sonic #1 (black) or sonic #2 (red). Damping correction either by ICO method (upper panel) or TEO (lower panel) during the overlapping period: Sep 30 – Oct. 1.

1.4 Discussion (extended)

1.4.1 Field performance

The miniDOAS system was steadily housed in an air-conditioned container, and was operational and measuring close to 100% of the campaign period. In the campaign, 35% of this time was spent on intercalibration of the two miniDOAS instruments, and the rest on flux measurements. Towards the end of the campaign, after the HT had been removed from the field, the miniDOAS instruments were intentionally kept in cross-setting for two extra weeks. These intercalibration measurements confirmed the baseline stability of the NH_3-difference measurements was better than 0.002 µg m^{-3} drift over a seven-week period. In future applications, the frequency and duration of the inter-instrumental calibration can be further optimized, increasing the percentage of operational flux measurements to well above 65%. The miniDOAS optical system was almost insensitive to degradation, although the parabola mirror and the lamp may need replacement after about a year. Hence, we conclude that the miniDOAS gradient setup is field ready in its current configuration, also for longer-term measurements.

For the HT, ~ 21% missing data were caused by raindrops or dew on the optical mirrors, and the coating material of the mirror gradually deteriorated along time over the five-week period presumably due to rain as well. In addition, the HT instrument needed regular operator intervention (e.g. mirror cleaning). To make the instrument suitable for longer-term monitoring, in particular in areas with frequent rainfall, this needs to be addressed in future versions.

1.4.2 Flexibility in application

For operation in the field, the miniDOAS system requires at least about 10 meter, preferably 20 meter, of relatively flat and horizontal surface between container and retroreflectors. It also requires structural stability to maintain the alignment between the miniDOAS instruments and their retroreflectors. That is feasible for ground-level operation but more difficult for a site with tall vegetation, for example when evaluating deposition above forest canopies from a tower. Besides, the miniDOAS instruments also need ~ 200 W at 230 V each, and are operated from a container ($2 \times 2 \times 2$ m) with air conditioning. Hence, its operation depends on a substantial mains power supply. The light-weight and portable HT instrument, on the other hand, currently only needs a 12 V, 50 W power supply permitting use at remote sites without access to mains power. It can be supported by a solar panel and a battery.

155 **Table S1. EddyPro basic settings for sonic#1, sonic #2, HT8700E and LI-7500DS.**

1. Metadata file	Canopy height	0.10 m					
1.1. Station	Displacement height	0.07 m					
	Roughness length	0.02 m					
1.2. Instruments		Anemometers Sonic#1	Gas Analyser info and their related distances to sonic #1		Anemometers Sonic#2	Gas Analyser info and their related distances to sonic #2	
	Manufacturer	Gill	LI-COR	Other Generic Open Path	Gill	LI-COR	Other Generic Open Path
	Model	Windmaster Pro	LI-7500DS	HT8700E	Windmaster	LI-7500DS	HT8700E
	Embedded software version	2329-105-01	8.8.36		2329-701-01	8.8.36	
	Instrument ID	Y071900			W211801		
	Height	2.80 m			2.80 m		
	Wind data format	U,V & W			U,V & W		
	North alignment	Spar			Spar		
	North off-set	40.0 °			320.0 °		
	Northward separation	Reference	-14.14 cm	-135.20 cm	Reference	95.46 cm	34.64 cm
	Eastward separation	Reference	14.14 cm	77.50 cm	Reference	-95.46 cm	-20.00 cm
	Vertical separation	Reference	3.00 cm	0.00 cm	Reference	0.00 cm	0.00 cm
	Longitudinal path length			50.00 cm			50.00 cm
	Transversal path length			10.00 cm			10.00 cm
	Time response			0.10 s			0.10 s

1.3(a). Raw File Description for sonic#1	1 ~ 4	5 ~ 6	7 ~ 8	9	10
Variable	u,v,w; sonic temperature	CO_2, H_2O	Ambient temperature and pressure	OSS	NH_3
Instrument	Sonic 1: Windmaster Pro	Irga 1: LI-7500DS	Irga 1: LI-7500DS	Irga 2: Generic Open Path	Irga 2: Generic Open Path
Measurement type		Molar/Mass density		Other	Molar/Mass density
Input unit	m/s; K	mmol/m^3	K; Pa	Dimensionless	µg/m^3
Nominal time log	0 s	0 s			
Minimum time log	0 s	-3.0 s	-3.0 s	-5.0 s	-5.0 s
Maximum time log	0 s	3.0 s	3.0 s	5.0 s	5.0 s

1.3(b). Raw File Description for sonic#2	1 ~ 4	5 ~ 6	7 ~ 8	9	10
Variable	u,v,w; sonic temperature	CO_2, H_2O	Ambient temperature and pressure	OSS	NH_3
Instrument	Sonic 2: Windmaster	Irga 1: LI-7500DS	Irga 1: LI-7500DS	Irga 2: Generic Open Path	Irga 2: Generic Open Path
Measurement type		Molar/Mass density		Other	Molar/Mass density
Input unit	m/s; K	$mmol/m^3$	K; Pa	Dimensionless	$\mu g/m^3$
Nominal time log	0 s	0 s			
Minimum time log	0 s	-5.0 s	-5.0 s	-3.0 s	-3.0 s
Maximum time log	0 s	5.0 s	5.0 s	3.0 s	3.0 s

2. Basic settings		
	Missing samples allowance:	40%
	Flux averaging interval:	30 min
	Cross wind correction of sonic temperature applied by the anemometer firmware:	Yes

3. Advanced settings		**Raw data processing for sonic #1**	**Raw data processing for sonic #2**
3.1 Processing options	Fix 'w boost' bug:	Yes	No
	Angle-of-attack correction for wind components:	Yes	Other settings are same as sonic #1
	Rotation method:	Double rotation	
	Detrend method:	Linear detrending	
	Time lag detection method:	Covariance maximization with default	
	Random uncertainty estimation:	Finkelstein and Sims(2001)	
		Cross-correlation first crossing 1/e	
		10.0 s	
	Flagging policy:	Mauder and Foken (2004)(0-1-2 system)	
3.2 Spectral Correction Options	Low frequency range:	Analytic correction of high-pass filtering effects (Moncrieff et al. 2004)	
	High frequency range:	Correction of low-pass filtering effects: Moncrieff et al. (1997) - Fully analytic	

Table S2: Number of AGM and EC NH_3 flux observations that were left after quality control steps.

	Filter criteria	AGM miniDOAS			EC HT		
		[nobs]	**[hours]**	**[%]**	**[nobs]**	**[hours]**	**[%]**
Total campaign duration		2283	1142	100%	1737	869	100 %
Gaps or intercalibration*		1491	746	65 %	1370	685	79 %
Filter 1	QF = 2	n/a	n/a	n/a	1229	615	71 %
Filter 2	u_*>0.1	1201	601	53 %	1035	517	60 %
Filter 3	2σ outlier filter	1193	597	52 %	1031	516	59 %
Filter 4	exclude 11-09-2022	1146	573	50 %	1002	501	58 %
Filter 5	both systems have flux	848	426	37 %	848	424	49 %
Wind sector	green	113	57	5 %	113	57	7 %
	lightgreen	115	58	5 %	115	58	7 %
	yellow	199	100	9 %	199	100	11 %
	red	421	211	18 %	421	211	24 %

**For the EC, data gaps were either weather-related and/or due to low optical signal strength (OSS). For the AGM, there were less observations due to the intercalibration of the miniDOAS instruments.*

1.5 References

Finkelstein, P. L. and Sims, P. F.: Sampling error in eddy correlation flux measurements, Journal of Geophysical Research, 106, 3503, https://doi.org/10.1029/2000JD900731, 2001.

LI-COR Inc: Using the LI-7500DS Open Path CO2/H2O Analyzer and SmartFlux 2 System, LI-COR Biosciences, Lincoln, 2022.

Mauder, M. and Foken, T.: Impact of post-field data processing on eddy covariance flux estimates and energy balance closure Meteorologische Zeitschrift, 15, 597-609, https://doi.org/10.1127/0941-2948/2006/0167, 2006.

Wolff, V., Trebs, I., Ammann, C., and Meixner, F. X.: Aerodynamic gradient measurements of the NH_3-HNO_3-$NH4NO_3$ triad using a wet chemical instrument: an analysis of precision requirements and flux errors, Atmos. Meas. Tech., 3, 187-208, https://www.doi.org/10.5194/amt-3-187-2010, 2010.